Investigating ^{6,7}Li-induced reactions on ^{235,238}U through a collective clusterization approach

Rupinder Kaur,[1,*] BirBikram Singh,[2] Maninder Kaur,[3] Manoj K. Sharma,[4] and Pushpendra P. Singh[5,†]

[1]*iHub - AWaDH, Indian Institute of Technology Rupnagar, Punjab 140001, India*
[2]*Department of Physics, Akal University, Talwandi Sabo, Punjab 151302, India*
[3]*Department of Physics, I.K.G. Punjab Technical University, Kapurthala 144603, India*
[4]*School of Physics and Materials Science, Thapar University, Patiala 147004, India*
[5]*Department of Physics, Indian Institute of Technology Rupnagar, Punjab 140001, India*

(Received 22 June 2023; accepted 23 August 2023; published 11 September 2023)

The characteristic cluster structures and low separation energies of weakly bound stable nuclei and their influence on the fusion process remain the subject of interest on experimental as well as theoretical fronts. To understand the fusion the dynamics of weekly bound nuclei, a comparison of fusion cross sections in reactions involving weakly bound projectiles ^{6,7}Li on ^{235,238}U targets was carried out within the collective clusterization approach of the dynamical cluster decay model (DCM) using deformed configuration effects included up to quadrupole deformations (β_{2i}) for two nuclei having optimum orientations $\theta^{\text{opt.}}$ at similar center-of-mass energies ($E_{\text{c.m.}}$). The fission excitation functions are tuned with respect to the available experimental data using the same neck length parameter (ΔR), the only free parameter in the model. Signatures of fusion enhancement and incomplete fusion (ICF) were observed at below-barrier energies, which is consistent with the experimental results. The plausible segregation of CF (complete fusion) and ICF was also made within the formalism.

DOI: 10.1103/PhysRevC.108.034611

I. INTRODUCTION

Over the past few decades, new technologies paved the way toward understanding complex phenomena involved in weakly bound stable and radioactive nuclei-induced reactions at sub- and above-barrier energies. Extensive experimental [1–11] and theoretical [12–14] investigations have been carried out to study the effect of breakup involving weakly bound projectiles on fusion. However, the findings still need to be supported with additional studies. Nuclear reactions involving weakly bound projectiles mainly result in two independent fusion processes, i.e., complete (CF) and incomplete fusion (ICF). In the case of CF, the projectile completely amalgamate with the target nuclei. In contrast, ICF is linked with splitting the projectile nuclei into its constituents before interacting with the target nuclei, of which only a part of the projectile fuses with the target nucleus, and the remnant goes in the forward direction nearly undeflected. The different possible reaction mechanisms to study the breakup fusion process and its influence on the fusion mechanism are discussed in Ref. [13]. Weakly bound nuclei, e.g., ^{6,7}Li and ^{9}Be involving $\alpha + x$ cluster structure with 1.48, 2.45, and 1.67 MeV separation energies, respectively, are considered the most suitable projectiles to investigate the role of breakup on the fusion mechanism. Apart from the characteristic cluster structure of these nuclei and their lower binding energies, a long tail in the density distribution affects the fusion process. Thus, a clear identification of these factors is necessary to compare theoretical predictions of experimental data involving complete and incomplete fusion reactions.

Based on theoretical underpinnings, some models [15] predict higher fusion cross sections in reactions involving weakly bound projectiles in comparison to the fusion resulting from tightly bound projectile induced reactions, and indicate weakly bound projectile breakup channels as the cause for such enhancement. In contrast, some models [16,17] indicate the hindrance in complete fusion due to the loss of incident flux caused by the projectile breakup. The findings of Ref. [12] suggest fusion enhancement at sub-barrier energies and fusion hindrance at above-barrier energies due to projectile breakup. Experimentally, many authors [18–20] claimed fusion enhancement at sub-barrier energies, whereas Refs. [21–23] suggest fusion suppression at above-barrier energies. In most of the experiments [1–4,6,9,19], only the total fusion cross section were measured, while in Refs. [7,8], the complete fusion component was distinguished from the incomplete fusion. Other investigations proposed that the study of fission involving weakly bound projectiles may provide a clearer picture of the structure and reaction dynamics of two interacting nuclei [24] because it can give important information about the formation cross section of the compound nucleus, fission barriers, and survival probabilities of these nuclei. Some studies have discussed the effect of projectile breakup on fission fragment (FF) angular anisotropy and fission fragment mass distribution [25–27] as well. However, FF angular anisotropy is also found to be affected by transfer-induced fission. Experimentally it is still difficult to

*Also at University School of Engineering, Lamrin Tech Skills University, Punjab 140001, India.
†pps@iitrpr.ac.in

 ©2023 American Physical Society

disentangle between the breakup and transfer-induced fission. Therefore, a systematic theoretical study of such systems will make it possible to predict CF and ICF cross sections and accomplish the challenging task of extricating the breakup and transfer-induced fusion.

With this motivation, we have chosen fissile systems ^{241,242,244,245}Am* for which experimental data are available in [27]. The present work conducts a comparative analysis concerning the CF and ICF to investigate the fusion enhancement at near-barrier energies. Through this investigation, an attempt was made to shed light on the impact of projectile breakup on fusion dynamics and to have better insight into segregating the CF and ICF processes. Further, the ER cross sections for the mentioned systems were also predicted. It is worth mentioning here that in the sub-barrier regime, where it is classically prohibited to fuse two nuclei, the fusion process can be achieved through quantum tunneling. The existing experimental data were reproduced for the specified energy range using the suitable neck length parameter ΔR at comparable $E_{\rm c.m.}$ values within the collective clusterization approach of the dynamical cluster-decay model (DCM), which is based on quantum mechanical fragmentation theory (QMFT). This model has been successfully applied to the loosely bound projectiles [28,29]. The study is organized as follows: Section II provides a brief overview of the dynamical cluster-decay model. The calculations and findings for excitation functions of CN under study are discussed in Sec. III. Finally, the results are summarized in Sec. IV.

II. DYNAMICAL CLUSTER-DECAY MODEL FOR HOT AND ROTATING COMPOUND SYSTEMS

The dynamical cluster-decay model is based on the quantum mechanical fragmentation theory [30]. This model is utilized successfully to do theoretical calculations in the light, medium, and heavy mass regions [31–38]. All possible decay mechanisms of the compound nucleus can be handled within the model, including emission of light particle (LPs), $A \leqslant 4$ (resulting in evaporation residues), intermediate mass fragments (IMFs), $5 \leqslant A \leqslant 20$, and fission fragments (FFs), $A/2 \pm 20$. In contrast to statistical models, it treats all fragmentation events on an equal footing as dynamical collective mass motion through the barrier with different quantum mechanical probabilities. As a result, it can describe the much-needed dynamical picture involved in the decay process. The calculations in the model are carried out in terms of two coordinates. The first coordinate is the collective coordinates of mass asymmetry (and charge asymmetry) [and $\eta_Z = (Z_1 - Z_2)/(Z_1 + Z_2)$], where the subscripts 1 and 2 stand for heavy and light fragments, respectively. The second is the relative separation coordinate R between two nuclei or, in general, between two fragments, which includes deformation effects from quadrupole to hexadecupole $\beta_{\lambda i}$ ($\lambda = 2, 3, 4$, $i = 1, 2$) and optimum orientation $\theta_i^{\rm opt.}$.

Here, the first coordinate η refers to the nucleon division (or exchange) between outgoing fragments. The separation coordinate R characterizes the transfer of kinetic energy of the incoming channel ($E_{\rm c.m.}$) to internal excitation [total excitation energy (TXE) or total kinetic energy (TKE)] of the outgoing channel. The CN decay cross section or the fragment production cross section can be defined in terms of these coordinates for different ℓ partial waves and is given as

$$\sigma = \sum_{\ell=0}^{\ell_{\rm max}} \sigma_\ell = \frac{\pi}{k^2} \sum_{\ell=0}^{\ell_{\rm max}} (2\ell + 1) P_0 P T_\ell, \quad k = \sqrt{\frac{2\mu E_{\rm c.m.}}{\hbar^2}}, \quad (1)$$

where T_ℓ is the entrance channel penetration probability, i.e., the CN formation probability $T_\ell = 1$ for $\ell \leqslant \ell_{\rm max}$ and zero for $\ell > \ell_{\rm max}$. The term P_0 is called preformation probability and refers to η motion. It provides significant information related to nuclear structure, and the term P known as penetrability refers to R motion. Generally, $\sigma_{\rm Fusion} = \sigma_{\rm ER} + \sigma_{\rm FF}$, where $\sigma_{\rm ER}$ and $\sigma_{\rm FF}$ are contributions towards total fusion cross section from evaporation residues, fusion-fission. For the chosen systems under investigation, the fusion cross section is observed to have a contribution from fission alone; however, as the model treats all the fragmentation processes on equal footing as the dynamical collective mass motion with different quantum mechanical probabilities through the barrier, as mentioned earlier we have calculated ER cross sections also along with fission. μ in Eq. (1) is referred as reduced mass ($\mu = \frac{A_1 A_2}{A_1 + A_2} m$), where m is the nucleon mass. $\ell_{\rm max}$ is known as the maximum angular momentum; it corresponds to the value of angular momentum ℓ for which $\sigma_{\rm ER}$ becomes negligibly small.

The preformation probability $P_0(A_i) = |\psi_R(\eta(A_i))|^2 \sqrt{B_{\eta\eta}} \frac{2}{A_{\rm CN}^*}$ of fragments inside the CN is given by the solution of the stationary Schrödinger wave equation in η, at fixed $R = R_a$,

$$\left\{ -\frac{\hbar^2}{2\sqrt{B}_{\eta\eta}} \frac{\partial}{\partial \eta} \frac{1}{\sqrt{B}_{\eta\eta}} \frac{\partial}{\partial \eta} + V(R, \eta, T) \right\} \psi^\nu(\eta) = E^\nu \psi^\nu(\eta) \quad (2)$$

with $\nu = 0, 1, 2, 3, \ldots$ referring to ground-state ($\nu = 0$) and excited-states ($\nu = 1, 2, 3, \ldots$) solutions and $i = 1$ or 2, for the heavy and light fragment, respectively, and assuming the Boltzmann-like occupation of excited states,

$$|\psi(\eta)|^2 = \sum_{\nu=0}^{\infty} |\psi^\nu(\eta)|^2 \exp(-E^\nu/T). \quad (3)$$

In Eq. (2) the mass parameters $B_{\eta\eta}$ are the classical hydrodynamical masses [39].

Here, for the spherical as well as deformed and oriented reaction products, the term R_a, which is defined as

$$R_a = R_1(\alpha_1, T) + R_2(\alpha_2, T) + \Delta R(T), \quad (4)$$

is the first turning point of the penetration path. For deformed and oriented nuclei the formalism is generalized by using the radii R_1 and R_2 and is given by

$$R_i(\alpha_i, T) = R_{0i}(T) \left[1 + \sum_\lambda \beta_{\lambda i} Y_\lambda^{(0)}(\alpha_i) \right]. \quad (5)$$

α_i is the angle between the symmetry axis and the radius vector of the interacting nucleus and is measured in the clockwise direction with respect to the symmetry axis. The

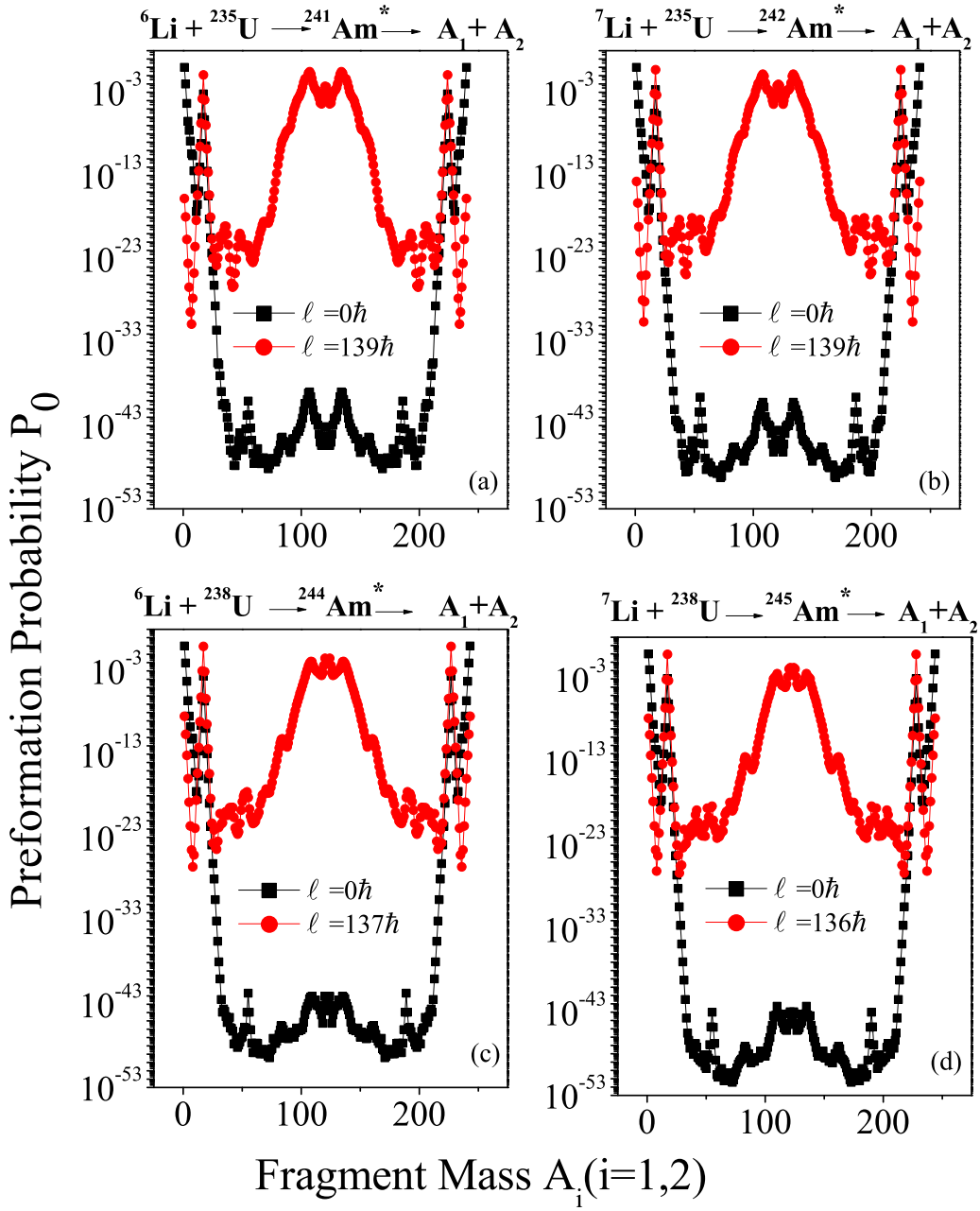

FIG. 1. The preformation probability P_0 as a function of fragment mass number A_i ($i = 1, 2$), calculated for two extreme ℓ values, for the CN ^{241,242,244,245}Am* at $E_{\text{c.m.}} \approx 27$ MeV for deformed fragmentation paths.

temperature-dependent nuclear radius $R_{0i}(T)$ for equivalent spherical nuclei is defined as $R_{0i}(T) = [1.28A_i^{1/3} - 0.76 + 0.8A_i^{-1/3}](1 + 0.0007T^2)$ [40], and T (in MeV) is related to $E^*_{\text{CN}} = \frac{1}{9}AT^2 - T = E_{\text{c.m.}} + Q_{\text{in}}$ where Q_{in} is the Q value of the incoming channel. In Eq. (4) ΔR is the temperature dependent neck length parameter that assimilates the neck formation effects between two nuclei, whose value remains within the range of validity (≈2 fm) of the proximity potential used here, and varies smoothly with temperature of the CN. The preformation probability, P_0, which is an important component of the model and contains the structure information of the CN, enters via the minimized fragmentation potential and is plotted in Figs. 1(a)–1(d). The fragmentation potential $[V_R(\eta, \ell, T)]$ for differently chosen CN is defined as

$$V(R, \eta, \ell, T) = \sum_{i=1}^{2}[V_{\text{LDM}}(A_i, Z_i, T)] + \sum_{i=1}^{2}[\delta U_i]\exp\left(-T^2/T_0^2\right) + V_C(R, Z_i, \beta_{\lambda i}, \theta_i, T) + V_P(R, A_i, \beta_{\lambda i}, \theta_i, T) + V_\ell(R, A_i, \beta_{\lambda i}, \theta_i, T). \quad (6)$$

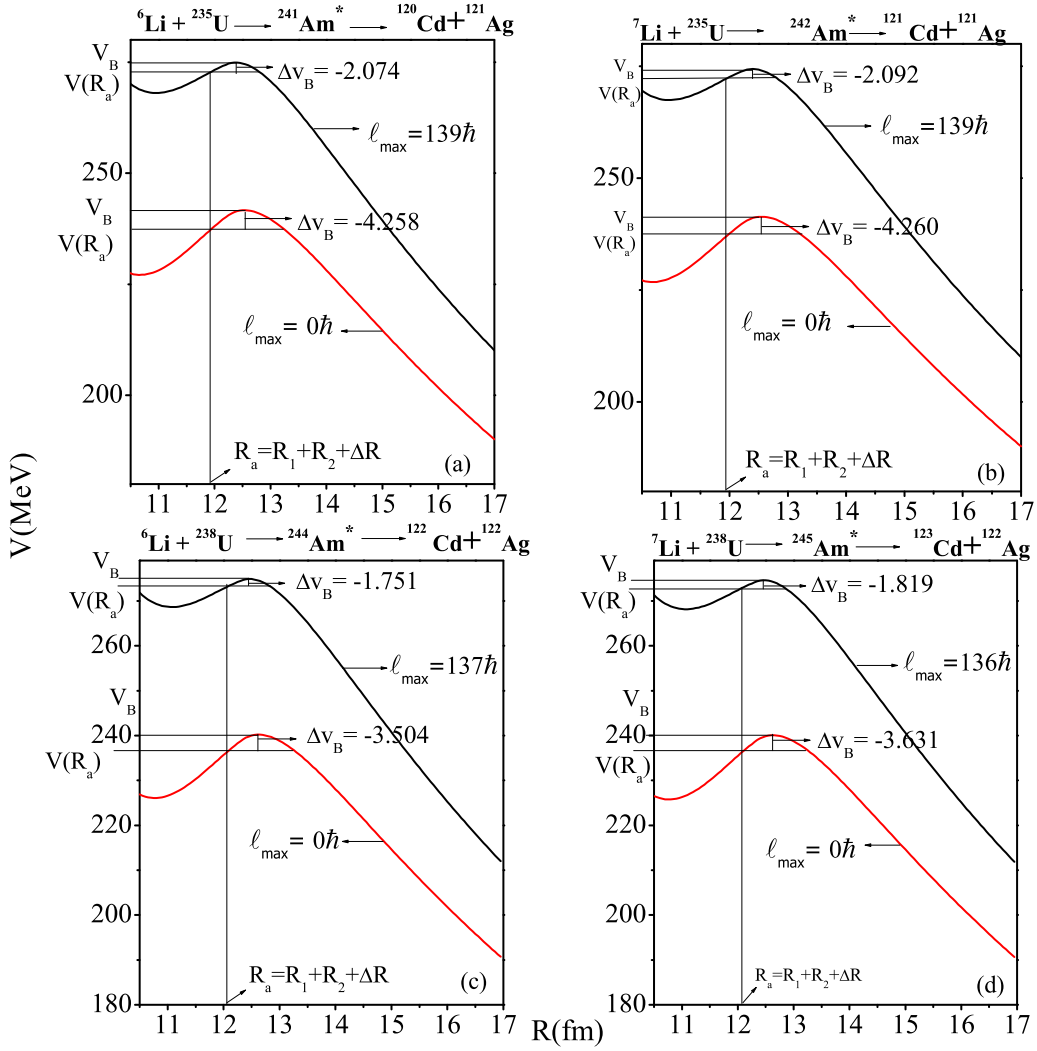

FIG. 2. The scattering potentials V, for the compound nuclei ^{241,242,244,245}Am* decaying through one of the probable exit channels at $E_{\text{c.m.}} \approx 27$ MeV for a set of extreme ℓ values.

In the fragmentation potential equation above, V_{LDM} is the T-dependent liquid drop model energy from Davidson *et al.* [41], and $\delta U(T)$ is the empirical shell correction from Myers and Swiatecki [42], which is also made T dependent to vanish exponentially with $T_0 = 1.5$ MeV [43]. V_C, V_P, and V_ℓ, respectively, are known as the T-dependent Coulomb potential, the nuclear proximity potential [44], and the centrifugal part of the interaction process. The Coulomb potential for the two interacting hot, deformed, and oriented nuclei is given by

$$V_C(R, Z_i, \beta_{\lambda i}, \theta_i, T) = Z_1 Z_2 e^2/R(T) + 3Z_1 Z_2 e^2 \times \sum \frac{R_i^\lambda(\alpha_i, T)}{(2\lambda+1)} Y_\lambda^{(0_i)} \left[\beta_{\lambda i} + \frac{4}{7}\beta_{\lambda i}^2 Y_\lambda^{(0)}(\theta_i)\right]. \quad (7)$$

The deformation parameters ($\beta_{\lambda i}$)of the nuclei are taken from the tables of Moller *et al.* [45]. $Y_\lambda^{(0)}(\theta_i)$ are the spherical harmonic functions, and the orientation angle (θ_i) is the angle between the nuclear symmetry axis and the collision Z axis and is measured in the counterclockwise direction. The term V_ℓ gives the centrifugal effects and are calculated by

$$V_\ell(R, A_i, \beta_{\lambda i}, \theta_i, T) = \hbar^2 \ell(\ell+1)/2I_s(T). \quad (8)$$

In the above expression $I_s(T)$ is the moment of inertia and is used in the sticking limit, which is more appropriate for the proximity potential (nuclear surface $\leqslant$2 fm), i.e.,

$$I = I_s(T) = \mu R^2 + \tfrac{2}{5}A_1 m R_1^2(\alpha_1, T) + \tfrac{2}{5}A_2 m R_2^2(\alpha_2, T). \quad (9)$$

Now, the term P, known as penetration probability (or the tunneling probability) used in calculating the cross section as given in Eq. (1), is calculated as the Wentzel-Kramers-Brillouin (WKB) tunneling probability,

$$P = \exp\left[\frac{-2}{\hbar}\int_{R_a}^{R_b}\sqrt{2\mu[V(R) - V(R_a)]}dR\right], \quad (10)$$

solved analytically [46]. The tunneling profile is shown in Figs. 2(a)–2(d). The first and second turning points satisfy

$$V(R_a) = V(R_b) = Q_{\text{eff}} = \text{TKE}(T). \quad (11)$$

Just like Q_{out} in the case of spontaneous ($T = 0$) cluster decay [31]. the potential $V(R_a)$ can be looked upon as the effective,

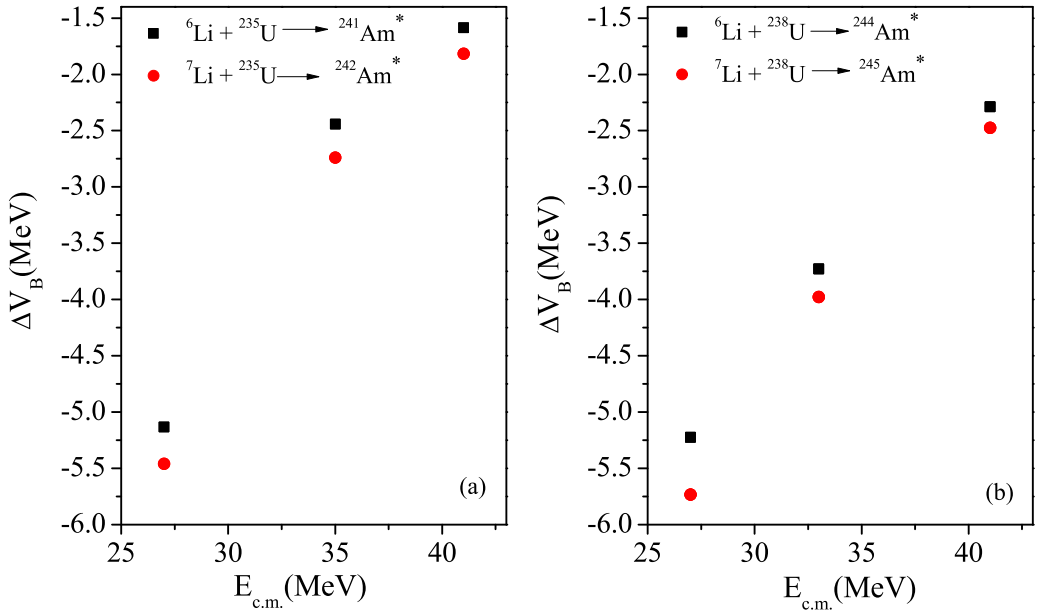

FIG. 3. The variation of the barrier lowering parameter ΔV_B as a function of ℓ for the compound nuclei ^{241,242,244,245}Am* for one of the probable exit channels.

positive Q value, $Q_{\rm eff}(T, \ell)$ [=TKE(T)], for the decay of the hot compound nucleus. Using Eq. (11), $R_b(\ell)$ is given by the ℓ-dependent scattering potential at fixed T,

$$V(R, T, \ell) = [Z_H Z_L e^2/R(T)] + V_P(T) + V_\ell(T), \qquad (12)$$

which is normalized to the exit channel binding energy. The choice of R_a [equivalently, ΔR in Eq. (4)] allows us to define, equivalently, the barrier lowering parameter, ΔV_B, which simply relates $V(R_a, \ell)$ and the top of the barrier $V_B(\ell)$, for each ℓ:

$$\Delta V_B = V(R_a, \ell) - V_B(\ell). \qquad (13)$$

Here, $V(R_a, \ell)$ and $V_B(\ell)$ represents the actual barrier used for the penetration and the top barrier position, respectively. This quantity of barrier lowering addresses the data in the below-barrier region to explain the observed hindrance phenomenon.

III. CALCULATIONS AND DISCUSSIONS

The analysis of heavy-ion-induced fusion reactions across the Coulomb barrier was performed within DCM for ^{6,7}Li + ^{235,238}U reactions populating compound nuclei (CN) ^{241,242,244,245}Am*. The calculations are performed by including deformation effects up to quadrupole deformation and with optimum orientations $\theta_i^{\rm opt.}$. The experimental fission cross sections ($\sigma_{\rm fiss}$) for all systems were reproduced by the using neck length parameter (ΔR) as a free parameter at similar $E_{\rm c.m.}$ values both below as well as above the Coulomb barrier. The same values of ΔR are used to fit fission excitation data for reactions involving the same target. Evaporation residue cross sections are also predicted for each reaction. With the inclusion of quadrupole deformation effects of two nuclei having optimum orientations and the effective lowering of the barrier (using the WKB quantum tunneling process), the cross sections of ^{7}Li-induced reactions are very well reproduced, indicating no ICF component, whereas, the data for ^{6}Li-induced reactions remain unaddressed, suggesting ICF content. Thus, we have also fitted the ICF component for both possible (^{2}H and ^{4}He) channels formed after the breakup of ^{6}Li. The DCM calculated cross sections show a nice agreement with the experimental data. This section describes the significance of the various parameters incorporated in the model to obtain the cross section and their importance in addressing the involved reaction mechanism of the CN.

A. Comparison of the effect of ^{6}Li and ^{7}Li on reaction dynamics

This part of the section focuses on the effect of ^{6}Li and ^{7}Li on reaction dynamics involving different targets. The structural information of the compound nucleus is provided by the preformation probability (P_0) which, as discussed earlier, is obtained from the calculated fragmentation potentials in the fragmentation process. P_0 is assigned to each minimized fragment in the fragmentation process.

To understand the probable structure of the decaying ^{241,242,244,245}Am* CN formed in the ^{6,7}Li + ^{235,238}U reactions, P_0 is estimated for various fragments/clusters created inside the CN. The calculated preformation probabilities in the decay of these CN are plotted at similar $E_{\rm c.m.}$ for extreme values of angular momenta, and are shown Figs. 1(a)–1(d). $\ell_{\rm max}$ is determined at the point where light particle (LP) cross section becomes negligibly small ($\sigma_{LP} \rightarrow 0$). Figures 1(a)–1(d) depict that at lower ℓ values LPs are dominating while at higher ℓ both fission and a few intermediate mass fragments (IMFs) compete for all the decaying CN. Although the IMFs show peaks in the preformation profile, the contribution towards the total cross section is negligible owing to low penetration probability values.

The tunneling of these energetically favored fragments through the barrier is determined through the scattering

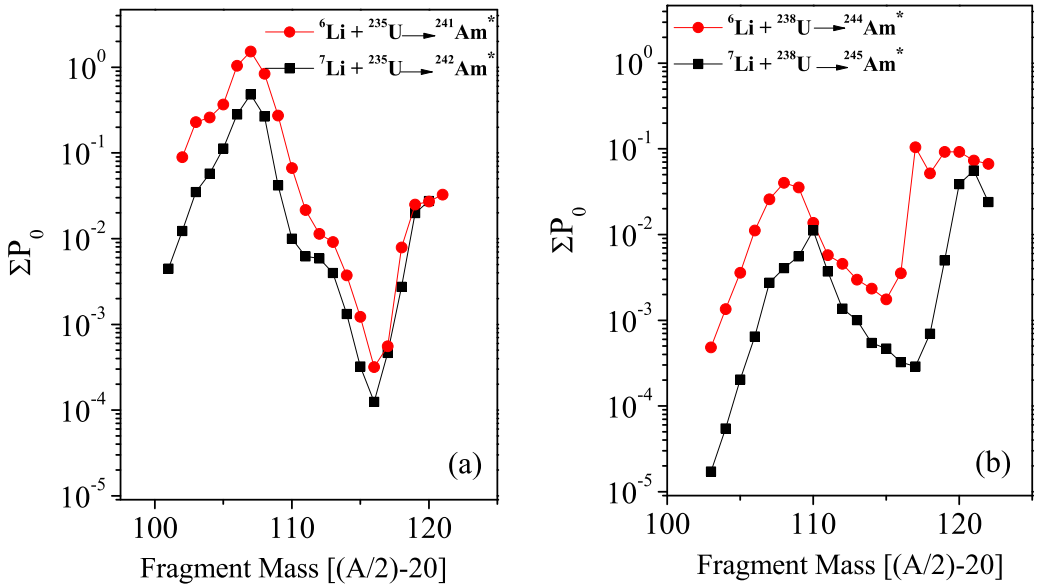

FIG. 4. The ℓ-summed up preformation probability as a function of fragment mass number (A_2) calculated for the compound nuclei ^{241,242,244,245}Am* at $E_{\text{c.m.}} \approx 27$ MeV.

potential and penetration probability of these fragments. The scattering potentials for all the CN, i.e., ^{241,242,244,245}Am* having $E_{\text{c.m.}} \approx 27$ MeV, decaying through one of the probable exit channels at extreme ℓ values, are shown in Figs. 2(a)–2(d). One of the important aspects of the model is its inbuilt property of barrier modification at near- and sub-barrier energies, which is depicted for the extreme values of angular momenta. In Figs. 2(a)–2(d) R_a correspond to the first turning points, for the respective exit channels of CN. It can be observed from the figure that the barrier lowering (ΔV_B) is maximum for $\ell = 0\hbar$ (lower lines), whereas it is minimum at ℓ_{max} (upper lines). The scattering potentials for different exit channels are used to calculate the penetration probability of the preformed fragments. In Figs. 3(a) and 3(b) the barrier lowering (ΔV_B) is plotted against $E_{\text{c.m.}}$ for all systems under observation. It indicates that the lowering of the barrier decreases with an increase in $E_{\text{c.m.}}$ for all the chosen CN, suggesting a lower cross section at sub-barrier energies. It is pointed out that the lowering of barrier values (ΔV_B) required in the case of ^{6}Li on ^{235,238}U is less than that of ^{7}Li on ^{235,238}U. Thus, the quantum tunneling of the fragments in the case of compound nuclei ^{241,244}Am* is less hindered than that of ^{242,245}Am*. Moreover, if we compare Figs. 3(a) and 3(b), it is inferred that overall barrier lowering is smaller in the case of the ^{6,7}Li reaction with ^{235}U, thereby resulting in enhanced cross-section values. This result is further explored through the ℓ summed P_0 values of the most favored outgoing fragments, as discussed below.

To investigate the role of these energetically favored fragments in the reaction dynamics, the variation of ℓ summed P_0 ($\sum P_0$) as a function of fragment mass is depicted in Figs. 4(a) and 4(b). It can be noted from Fig. 4(a) that $\sum P_0$ is greater for preformed fission fragments of the induced reaction of ^{6}Li on ^{235}U in comparison to the reaction ^{7}Li on ^{235}U. Similar behavior is observed for the systems ^{6}Li on ^{238}U and ^{7}Li on ^{238}U, as shown in Fig. 4(b). It is deduced from these plots that ℓ summed P_0 are in general greater for the fission fragments of ^{6,7}Li on ^{235}U reactions than that of preformed fission frag-

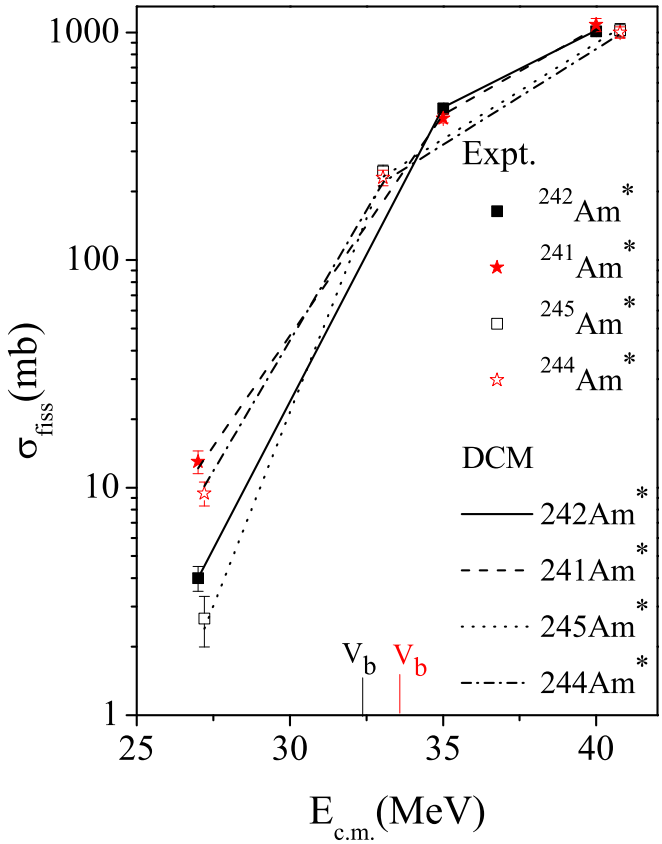

FIG. 5. The fission cross section, σ_{fiss} calculated at comparable center-of-mass energies for ^{241,242,244,245}Am* within DCM and are compared with available experimental data for deformed fragmentation.

TABLE I. The DCM-calculated (CF) fission cross section $\sigma_{\rm fiss}$ and predicted ER cross section $\sigma_{\rm ER}$ considering the deformed fragmentation path and compared with experimental data [27] for CN ^{241,242,244,245}Am* at similar $E_{\rm c.m.}$ values.

					Expt.	DCM$_{\rm CF}$ (mb)	
Reaction	$E_{\rm c.m.}$ (MeV)	T (MeV)	$\ell_{\rm max}$ ($\hbar$)	ΔR (fm)	$\sigma_{\rm fiss}$ (mb)	$\sigma_{\rm ER}$	$\sigma_{\rm fiss}$
^{6}Li + ^{235}U → ^{241}Am*	27	1.061	139	0.97	13 ± 1.5	1.17×10^{-6}	7
	35	1.195	140	1.2	419.5 ± 19	0.034	436
	40.96	1.2734	143	1.28	1080 ± 73	0.18	1102
^{7}Li + ^{235}U → ^{242}Am*	27	1.0283	139	0.97	4 ± 0.5	3.1×10^{-7}	4
	35	1.167	140	1.2	463.5 ± 26	0.044	468
	40.79	1.244	142	1.28	1010 ± 46	0.22	1020
^{6}Li + ^{238}U → ^{244}Am*	27.27	1.049	137	1.02	9.434 ± 1.135	1.06×10^{-5}	4
	33.14	1.1496	138	1.128	230 ± 18	0.014	220
	41.01	1.271	144	1.245	1000 ± 56.6	0.174	985
^{7}Li + ^{238}U → ^{245}Am*	27.21	1.0239	136	1.02	2.66 ± 0.663	2.7×10^{-6}	2.4
	33.04	1.1255	140	1.128	245 ± 16.6	9.1×10^{-3}	232
	40.78	1.2475	144	1.245	1024 ± 69.5	0.161	1046

ments of ^{6,7}Li on ^{238}U systems [which can be noticed from preformation probability profiles also, Figs. 1(a)–1(d)]. These higher values of $\sum P_0$ result in larger cross-section values of respective fragments. It is so because the cross sections follow the behavior of $\sum P_0$; that is, the highly performed fragment contributes the most towards the cross section (noted in earlier works also [36]). Hence, it is established that fusion enhancement resulting from higher values of $\sum P_0$ is larger for ^{6}Li-induced reactions than ^{7}Li on the same target nucleus. Moreover, when we compare ^{6}Li reactions with different target nuclei, it is observed that $\sum P_0$ is higher when ^{6}Li fuses with a lower mass of target nucleus (^{235}U) in comparison to a higher one (^{238}U). Similar behavior is observed when ^{7}Li is used as a projectile.

Finally, the calculated fission excitation values for all CN under study are plotted as a function of $E_{\rm c.m.}$ in Fig. 5. V_b depicted in black and red are the approximate Coulomb barriers for ^{6,7}Li on ^{235}U and ^{6,7}Li on ^{238}U, respectively. Fission cross sections for ^{6,7}Li + ^{235,238}U reactions at above-barrier energies are found to be almost similar. However, at sub-barrier energy, DCM calculated fission cross sections (CF+ICF) for ^{6}Li-induced reactions (represented by black dashed and dash-dotted lines) are much higher than those for ^{7}Li-induced reactions (represented by black solid and dotted lines). These findings are in accordance with the experimental results. It is important to mention here that this observation finds its roots in the collective clusterization approach of DCM explored in the above-mentioned discussion of Figs. 1(a)–1(d) and 4(a) and 4(b), for the present work.

B. Segregation of CF and ICF in ^{6}Li-induced reactions

The DCM calculated $\sigma_{\rm fiss}$ at similar $E_{\rm c.m.}$ values for β_2-deformed configurations for CF are given in Table. I, along with the experimental data at the reported energies. The predicted light particle cross section ($\sigma_{\rm ER}$) values at different energy points for all compound nuclei ^{241,242,244,245}Am* are also mentioned in the table. These predicted light particle cross sections show that fission dominates for these reactions. The $\ell_{\rm max}$ and ΔR values along with the temperature used in the calculations for all the systems are also given. The same ΔR values are used to reproduce and predict the experimental cross sections at similar $E_{\rm c.m.}$ values, consistent with Ref. [35].

The missing cross-section value (which we are not able to reproduce in CF as mentioned in Table I at the lowest energy point) is calculated for the case of the ^{6}Li-induced reaction. As the projectile ^{6}Li is a loosely bound nucleus and has small binding energy, it breaks into ^{4}He and ^{2}H, which results in ICF. The energies of the resulting new projectile are modified for the calculations as per Ref. [28]. The ICF calculated cross sections as reported in Table II show that the fission resulting from the fusion of the ^{4}He projectile is higher. Thus, we attempted to separate the CF and ICF components from the

TABLE II. The DCM-calculated ICF cross section for ^{6}Li-induced reactions, considering the deformed fragmentation path.

					DCM$_{\rm ICF}$ (mb)	
Reaction	$E_{\rm c.m.}$ (MeV)	T (MeV)	$\ell_{\rm max}$ ($\hbar$)	ΔR (fm)	$\sigma_{\rm ER}$	$\sigma_{\rm fiss}$
^{4}He + ^{235}U → ^{239}Pu*	18.33	0.721	118	1.02	6.68×10^{-8}	5.4
^{2}H + ^{235}U → ^{237}Np*	9.162	0.854	118	1.02	3.03×10^{-6}	0.73
^{4}He + ^{238}U → ^{242}Pu*	18.33	0.725	121	1.06	3.56×10^{-8}	4.66
^{2}H + ^{238}U → ^{240}Np*	9.242	0.826	121	1.06	1.64×10^{-6}	0.5

total cross-section value within the clusterization approach of DCM.

IV. SUMMARY

In the present work, the influence of weakly bound nuclei on reaction dynamics was carried out for ^{6,7}Li on ^{235,238}U reactions within the collective clusterization approach of the dynamical cluster decay mode (DCM) using deformed configuration effects including up to quadrupole deformations (β_{2i}) for two nuclei having optimum orientations $\theta^{\text{opt.}}$. The calculations are performed at similar center-of-mass energies ($E_{\text{c.m.}}$) both above and below the Coulomb barrier. The available experimental fission data for these CN were reproduced using neck length parameter ΔR, the only variable parameter of DCM, at similar $E_{\text{c.m.}}$ values. The model is also used to predict the ERs cross sections (σ_{ER}), which are found to contribute negligibly towards the total cross section; thus it is pointed out that, for the present reactions, fusion-fission cross section dominates.

Furthermore, it is conjectured that the greater values of $\sum P_0$ result in enhanced cross section of ^{6}Li-induced reactions in comparison to ^{7}Li on the same target nucleus. Overall, ^{6,7}Li on ^{235}U resulted in more enhanced cross section owing to their greater $\sum P_0$ values in comparison to the ^{6,7}Li on ^{238}U reaction. In addition, the barrier modification required for ^{6,7}Li-induced reaction on ^{235}U is less than that for ^{6,7}Li on ^{238}U target. This indicates that the quantum tunneling of the fragments in the case of compound nuclei ^{241,242}Am* is less hindered than that of ^{244,244}Am*, thereby resulting in enhanced cross-section values. Tables I and II give the details of the attempt made within DCM to segregate CF and ICF components. It is found that the fusion probability of ^{4}He in ICF is higher. DCM calculated cross sections are in nice agreement with the experimental data.

ACKNOWLEDGMENTS

One of the authors, R.K., would like to thank iHub-AWaDH established in the framework of the National Mission on Cyber-Physical Systems (NM-ICPS) by the Department of Science & Technology (DST), Government of India, at the Indian Institute of Technology Ropar, for support.

[1] A. Yoshida, C. Signorini, T. Fukuda, Y. Watanabe, N. Aoi, M. Hirai, M. Ishihara, H. Kobinata *et al.*, Phys. Lett. B **389**, 457 (1996).
[2] J. Takahashi, M. Munhoz, E. M. Szanto, N. Carlin, N. Added, A. A. P. Suaide, M. M. de Moura, R. Liguori Neto *et al.*, Phys. Rev. Lett. **78**, 30 (1997).
[3] J. J. Kolata, Eur. Phys. J. A Hadrons and Nuclei **13**, 117 (2002).
[4] I. Padron, P. R. S. Gomes, R. M. Anjos, J. Lubian, C. Muri, J. J. S. Alves, G. V. Martí, M. Ramírez *et al.*, Phys. Rev. C **66**, 044608 (2002).
[5] M. Trotta, J. L. Sida, N. Alamanos, A. Andreyev, F. Auger, D. L. Balabanski, C. Borcea, and N. Coulier, Phys. Rev. Lett. **84**, 2342 (2000).
[6] A. Mukherjee and B. Dasmahapatra, Phys. Rev. C **63**, 017604 (2000).
[7] M. Dasgupta *et al.*, Phys. Rev. Lett. **82**, 1395 (1999); Phys. Rev. C **66**, 041602(R) (2002).
[8] V. Tripathi, A. Navin, K. Mahata, K. Ramachandran, A. Chatterjee, and S. Kailas, Phys. Rev. Lett. **88**, 172701 (2002).
[9] C. Beck, F. A. Souza, N. Rowley, S. J. Sanders, N. Aissaoui, E. E. Alonso, P. Bednarczyk, N. Carlin *et al.*, Phys. Rev. C **67**, 054602 (2003).
[10] R. N. Sahoo, M. Kaushik, A. Sood, A. Sharma, S. Thakur, P. Kumar, M. M. Shaikh, R. Biswas, A. Yadav, M. K. Sharma, J. Gehlot, S. Nath, N. Madhavan, R. G. Pillay, E. M. Kozulin, G. N. Knyazheva, K. V. Novikov, and P. P. Singh, Phys. Rev. C **102**, 024615 (2020).
[11] M. Kaushik *et al.*, Phys. Rev. C **101**, 034611 (2020); **104**, 024615 (2021).
[12] K. Hagino, A. Vitturi, C. H. Dasso, and S. M. Lenzi, Phys. Rev. C **61**, 037602 (2000).
[13] A. Diaz-Torres and I. J. Thompson, Phys. Rev. C **65**, 024606 (2002); A. Diaz-Torres, I. J. Thompson, and W. Scheid, Nucl. Phys. A **703**, 83 (2002); Phys. Lett. B **533**, 265 (2002).
[14] N. Keeley, K. W. Kemper, and K. Rusek, Phys. Rev. C **65**, 014601 (2001); **66**, 044605 (2002).
[15] C. H. Dasso and A. Vitturi, Phys. Rev. C **50**, R12(R) (1994); C. H. Dasso, J. L. Guisado, S. M. Lenzi, and A. Vitturi, Nucl. Phys. A **597**, 473 (1996).
[16] N. Takigawa, M. Kuratani, and H. Sagawa, Phys. Rev. C **47**, R2470(R) (1993).
[17] M. S. Hussein, M. P. Pato, L. F. Canto, and R. Donangelo, Phys. Rev. C **46**, 377 (1992); **47**, 2398 (1993).
[18] C. H. Dasso and R. Donangelo, Phys. Lett. B **276**, 1 (1992).
[19] E. F. Aguilera, J. J. Kolata, F. D. Becchetti, P. A. DeYoung, J. D. Hinnefeld, A. Horvàth, L. O. Lamm, H.-Y. Lee *et al.*, Phys. Rev. C **63**, 061603(R) (2001).
[20] J. J. Kolata, V. Guimarães, D. Peterson, P. Santi, R. White-Stevens, P. A. DeYoung, G. F. Peaslee, B. Hughey *et al.*, Phys. Rev. Lett. **81**, 4580 (1998).
[21] N. Takigawa and H. Sagawa, Phys. Lett. B **265**, 23 (1991).
[22] M. S. Hussein, M. P. Pato, and A. F. R. de Toledo Piza, Phys. Rev. C **51**, 846 (1995).
[23] L. F. Canto, R. Donangelo, P. Lotti, and M. S. Hussein, Phys. Rev. C **52**, R2848(R) (1995).
[24] S. Kailas, Phys. Rep. **284**, 381 (1997).
[25] H. Freiesleben, G. T. Rizzo, and J. R. Huizenga, Phys. Rev. C **12**, 42 (1975).
[26] I. M. Itkis, A. A. Bogachev, A. Yu. Chizhov, D. M. Gorodisskiy, M. G. Itkis, G. N. Knyazheva, N. A. Kondratiev, E. M. Kozulin *et al.*, Phys. Lett. B **640**, 23 (2006).
[27] A. Parihari, S. Santra, A. Pal, N. L. Singh, K. Mahata, B. K. Nayak, R. Tripathi, K. Ramachandran *et al.*, Phys. Rev. C **90**, 014603 (2014).
[28] G. Kaur and M. K. Sharma, Nucl. Phys. A **884**, 36 (2012).
[29] M. S. Gautam, N. Grover, and M. K. Sharma, Eur. Phys. J. A **53**, 12 (2017).
[30] R. K. Gupta *et al.*, Phys. Rev. Lett. **35**, 353 (1975); A. Sandulescu *et al.*, Phys. Lett. B **35**, 225 (1976); R. K. Gupta *et al.*, *ibid.* **67**, 257 (1977).

[31] R. K. Gupta, M. Balasubramaniam, R. Kumar, D. Singh, C. Beck, and W. Greiner, Phys. Rev. C **71**, 014601 (2005).
[32] R. K. Gupta, M. Balasubramaniam, R. Kumar, D. Singh, C. Beck, and W. Greiner, J. Phys. G: Nucl. Part. Phys. **32**, 345 (2006).
[33] B. B. Singh, M. K. Sharma, and R. K. Gupta, Phys. Rev. C **77**, 054613 (2008).
[34] M. K. Sharma, S. Kanwar, G. Sawhney, and R. K. Gupta, Phys. Rev. C **85**, 064602 (2012).
[35] M. Kaur, B. Singh, M. K. Sharma, and Raj K. Gupta, Phys. Rev. C **92**, 024623 (2015); R. Kaur, M. Kaur, V. Singh, S. Kaur, B. Singh, and B. S. Sandhu, *ibid.* **98**, 064612 (2018).
[36] R. Kaur, S. Kaur, B. Singh, B. S. Sandhu, and S. K. Patra, Phys. Rev. C **101**, 034614 (2020); R. Kaur, M. Kaur, V. Singh, and M. Kaur, B. Singh, and B. S. Sandhu, *ibid.* **101**, 044605 (2020).
[37] S. Kaur, R. Kaur, B. Singh, and S. K. Patra, Nucl. Phys. A **1018**, 122361 (2022).
[38] S. Jain, Raj Kumar, S. K. Patra, and Manoj K. Sharma, Phys. Rev. C **105**, 034605 (2022).
[39] H. Kröger and W. Scheid, J. Phys. G **6**, L85 (1980).
[40] G. Royer and J. Mignen, J. Phys. G: Nucl. Part. Phys. **18**, 1781 (1992).
[41] N. J. Davidson, S. S. Hsiao, J. Markram, H. G. Miller, and Y. Tzeng, Nucl. Phys. A **570**, 61 (1994).
[42] W. Myers and W. J. Swiatecki, Nucl. Phys. **81**, 1 (1966).
[43] A. S. Jensen and J. Damgaard, Nucl. Phys. A **203**, 578 (1973).
[44] J. Blocki, J. Randrup, W. J. Swiatecki, and C. F. Tsang, Ann. Phys. **105**, 427 (1977).
[45] P. Moller, J. R. Nix, W. D. Myers, and W. J. Swiatecki, At. Data Nucl. Data Tables **59**, 185 (1995).
[46] S. S. Malik and R. K. Gupta, Phys. Rev. C **39**, 1992 (1989).